Journal of Applied Physics

RESEARCH ARTICLE | DECEMBER 06 2022

Electron effective masses of $Sc_xAl_{1-x}N$ and $Al_xGa_{1-x}N$ from first-principles calculations of unfolded band structure

Luigi Balestra ; Elena Gnani ; Susanna Reggiani

Journal of Applied Physics 132, 215108 (2022)
https://doi.org/10.1063/5.0115512

CrossMark
View Online
Export Citation

Articles You May Be Interested In

Microstructure and dielectric properties of piezoelectric magnetron sputtered w-$Sc_xAl_{1-x}N$ thin films

Journal of Applied Physics (May 2012)

Electron accumulation and distribution at interfaces of hexagonal $Sc_xAl_{1-x}N$/GaN- and $Sc_xAl_{1-x}N$/InN-heterostructures

Journal of Applied Physics (June 2022)

Non-leaky longitudinal acoustic modes in $Sc_xAl_{1-x}N$/sapphire structure for high-temperature sensor applications

Appl. Phys. Lett. (August 2019)

AIP Publishing

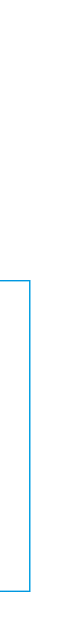
Downloaded from http://pubs.aip.org/aip/jap/article-pdf/doi/10.1063/5.0115512/16521706/215108_1_online.pdf

Journal of Applied Physics ARTICLE scitation.org/journal/jap

Electron effective masses of $Sc_xAl_{1-x}N$ and $Al_xGa_{1-x}N$ from first-principles calculations of unfolded band structure

Cite as: J. Appl. Phys. **132**, 215108 (2022); doi: 10.1063/5.0115512
Submitted: 27 July 2022 · Accepted: 5 November 2022 ·
Published Online: 6 December 2022

Luigi Balestra,[1,2,a)] Elena Gnani,[1,2] and Susanna Reggiani[1,2]

AFFILIATIONS

[1]Advanced Research Center on Electronic Systems "E. De Castro" (ARCES), University of Bologna, IT-40136 Bologna, Italy
[2]Department of Electrical, Electronic, and Information Engineering (DEI), University of Bologna, IT-40136 Bologna, Italy

[a)]**Author to whom correspondence should be addressed:** luigi.balestra5@unibo.it

ABSTRACT

The electron effective masses of $Sc_xAl_{1-x}N$ and $Al_xGa_{1-x}N$, two of the most promising wide bandgap materials for power and RF electronic applications, have been calculated using the predictions of the density functional theory (DFT). More specifically, the unfolding technique has been adopted to extract the effective band structure of the two alloys under investigation. It has been found that the AlGaN effective masses m^* approximately follow the Vegard law. On the contrary, due to the larger amount of disorder inside the crystal, the ScAlN shows a non-monotonic change of m^* as a function of the Sc concentration, which requires the DFT calculations to be consistently performed for an accurate prediction. The ScAlN effective masses as a function of Sc content have been reported in the range $0 \leq x \leq 0.25$ for the first time.

© 2022 Author(s). All article content, except where otherwise noted, is licensed under a Creative Commons Attribution (CC BY) license (http://creativecommons.org/licenses/by/4.0/). https://doi.org/10.1063/5.0115512

I. INTRODUCTION

Ultrawide-bandgap nitride materials are nowadays extensively used to produce electronic devices with high power density and efficiency when compared to their silicon counterparts. Actually, high electron mobility transistors (HEMTs) based on AlGaN/GaN heterostructures are widely studied because of their very promising electron concentration in the 2D electron gas (2DEG) ($1-2\times10^{13}\,\mathrm{cm}^{-2}$) and very high electron mobility ($10.000\,\mathrm{cm}^2/\mathrm{V/s}$).[1] The advantageous high 2DEG concentrations are due to the spontaneous and piezoelectric polarization in the AlGaN/GaN heterostructure. In the last few years, ScAlN, a scandium-based alloy, has been proposed as a substitute of the AlGaN for the next HEMT generation due to its superior material properties, such as the 3× higher spontaneous polarization.[2] As shown by Hardy *et al.*,[3] this results in 2DEG concentrations of $3.4\times10^{13}\,\mathrm{cm}^{-2}$. Moreover, ScAlN-based HEMT prototypes have been recently manufactured confirming theoretical predictions.[4,5] The phenomena that dominate on the charge transport in such devices can be accurately described by performing TCAD simulations, relying on the solution of the drift–diffusion model in a discrete domain and accounting for the main features of heterostructures and polarization. To this purpose, the transport model needs to be specialized also for the ScAlN material using a specific set of physical models and parameters. As a starting point, the ScAlN energy structure is needed to correctly account for the energy gap (Eg) and the density of states through the effective masses (m^*), adopted when assuming a parabolic dispersion relation $E(\boldsymbol{k})$ close to the conduction band minimum. The parabolic band is expressed as

$$E(\boldsymbol{k}) = \frac{\hbar^2 k^2}{2m^*}, \tag{1}$$

where $\hbar$ is the reduced Plank constant and $\boldsymbol{k}$ is the wave vector. From Eq. (1), the density of states (DOS) can be analytically calculated.[6] Such quantity provides the amount of free charges in the bulk and their temperature dependency. When treating alloys, such as AlGaN and ScAlN, supercells (SCs) are needed to properly take into account the random distribution of atoms inside the lattice. However, by performing density functional theory (DFT) simulations using SCs, the number of energy eigenvalues becomes proportional to the SC size, leading to a much more complex band structure, which needs to be treated with appropriate techniques.

Downloaded from http://pubs.aip.org/aip/jap/article-pdf/doi/10.1063/5.0115512/16521706/215108_1_online.pdf

© Author(s) 2022

To this purpose, the unfolding technique has been developed to map the energy eigenvalues obtained from SC calculations into an effective band structure (EBS) recovering an approximate dispersion relation $E(\boldsymbol{k})$, which collects the main features of the alloy properties.[7–9] Recently, it has been adopted to extract the electron effective mass of the lowest-lying conduction band close to the Γ point of $Al_{0.5}Ga_{0.5}N$.[10] Despite DFT simulations of ScAlN SCs were recently performed by Zhang *et al.*,[11] the effects of the Sc incorporation on the low energy transport properties have not been clarified yet. In this work, for the first time, the electron effective masses of ScAlN and AlGaN have been extracted for different values of the mole fraction x using the EBS. The analysis confirms that the ScAlN alloy shows a much more complex structure with respect to AlGaN due to the rock-salt configuration of the ScN that mixes with the AlN wurtzite structure. The reported results are fundamental in order to extend the future TCAD analysis to such kind of new material.

II. CALCULATION METHODS

The electronic properties of ScAlN and AlGaN have been calculated using the density functional theory (DFT) via the Quantum ESPRESSO (QE) package.[12] Norm-conserving (NC) pseudo-potential has been employed with the energy cut-off fixed to 100Ry. A $8 \times 8 \times 8$ Monkhorst–Pack grid has been used to sample the Brillouin zone of the wurtzite AlN (w-AlN) and wurtzite GaN (w-GaN) primitive cells (PCs). For the SC self-consistent calculations, a $4 \times 4 \times 4$ k-point grid has been used. The general gradient approximation (GGA) as parameterized by Perdew, Burke, and Ernzerhof (PBE)[13] has been adopted for the variable-cell relaxation. The lowest energy configuration has been achieved with all forces smaller than 0.001 Ry/aB and the pressure below 0.5 kbar.

In order to emulate the random position of Sc and Al atoms in the alloy, the special quasi-random structure (SQS) technique has been employed. More specifically, the Monte Carlo algorithm implemented in the Alloy Theoretic Automatic Toolkit (ATAT)[14] has been used to generate $2 \times 2 \times 2$ supercells containing a total number of 32 atoms, 16 of nitrogen and 16 of alloy atoms mixed with different concentrations.

Starting from the self-consistent solutions of the Kohn–Sham equations, the unfolding technique has been used to construct the EBS of both $Sc_xAl_{1-x}N$ and $Al_xGa_{1-x}N$ for different values of x. To ensure the quality of the unfolding procedure around the Γ point, the values of the spectral weights have been checked. They are defined as[8]

$$P_{\vec{K}m}(\vec{k}_i) = \sum_n |\vec{K}m|\vec{k}_i n|^2, \tag{2}$$

where m and n correspond to band indices, while $\vec{k}$ and $\vec{K}$ are wave vectors of the PC and the SC, respectively. This quantity represents the amount of Bloch character $\vec{k}_i$ preserved in $\left|\vec{K}m\right\rangle$ at $E_n = E_m$. If the SC is obtained by repeating identical PCs, the spectral weights reduce to

$$P_{\vec{K}m}(\vec{k}_i) = g_n(\vec{k}_i)\delta(E_m - E_n), \tag{3}$$

where $g_n(\vec{k}_i)$ is the bulk degeneracy of the PC state $\left|\vec{K}_i n\right\rangle$ at E_n. In w-AlN and w-GaN supercells, $P_{\vec{K}m}(\vec{k}_i) = 1$ at each eigenvalue $E_n(\vec{k}_i)$ of the PC, 0 otherwise. When considering pseudo-binary alloys, the spectral weights are no more δ functions. However, if the perturbation to the crystal symmetry is small, the spectral weights corresponding to the lowest-lying conduction band around the Γ point are still close to 1. Under such assumptions, the effective masses can be calculated by fitting the DFT bands around the minimum of the conduction band against the Kane model for non-parabolic spherical bands, which gives more accurate results when compared to Eq. (1). It reads

$$\varepsilon(1 + \alpha\varepsilon) = \frac{\hbar^2 k^2}{2m^*}. \tag{4}$$

As the energetic minimum is characterized by an ellipsoidal shape, the electron effective mass can be calculated by analyzing the band structure near Γ along the A direction ($m^{\parallel}$, parallel to the c direction of the crystal) and along the M and K directions ($m^{\perp}$, perpendicular to the c direction). It has been confirmed that the electron effective mass in the M and K directions is equal.[15] Thus, $m^* = (m^{\perp}m^{\perp}m^{\parallel})^{1/3}$ is the corresponding DOS effective mass.[6] The ScAlN DOS has been calculated integrating the Brillouin zone on an $8 \times 8 \times 8$ k-point grid adopting the tetrahedron method.[16]

III. SIMULATIONS OF BULK w-AlN AND w-cGaN

DFT simulations of bulk GaN and AlN have been performed to choose the most suitable approximations for the exchange-correlation potential. Lattice parameters of w-AlN and w-GaN, resulting from structural optimization, are in nice agreement with previous works based on GGA-PBE simulations and experiments as reported in Table I. For the sake of comparison, starting from the relaxed structure obtained from PBE, the following exchange correlation potential has been tested to calculate the electronic properties of the materials: the GGA-PBE potential used for relaxation, the modified Becke–Johnson (mBJ) with default parameters (which, in the QE package, is implemented only for norm-conserving pseudo-potential), and the hybrid pseudo-potential as defined by Heyd–Scuseria–Ernzerhof (HSE)[17] with a $4 \times 4 \times 4$ q-point grid. In the latter case, the Wannier90 code[18] has been

TABLE I. Lattice constants of w-GaN and w-AlN obtained from variable-cell relaxation.

		a (Å)	c (Å)	u (Å)
w-GaN	PBE (this work)	3.2129	5.2332	0.3770
	PBE (Ref. 11)	3.244	5.276	0.377
	PBE (Ref. 19)	3.210	5.232	0.377
	Exp. (Ref. 19)	3.19	5.200	0.377
w-AlN	PBE (this work)	3.1269	5.0129	0.3817
	PBE (Ref. 11)	3.125	5.010	0.382
	PBE (Ref. 19)	3.13	5.039	0.381
	Exp. (Ref. 19)	3.11	4.97	0.382

Downloaded from http://pubs.aip.org/aip/jap/article-pdf/doi/10.1063/5.0115512/16521706/215108_1_online.pdf

© Author(s) 2022

TABLE II. Calculated energy gap and electron effective masses of w-GaN and w-AlN.

		E_g (eV)	$m^{\perp}$ (m_0)	$m^{\parallel}$ (m_0)
w-GaN	PBE (this work)	1.76	0.17	0.15
	PBE $2 \times 2 \times 2$ SC (this work)	1.76	0.17	0.15
	PBE (Ref. 11)	1.58	n.a.	n.a.
	PBE (Ref. 20)	n.a.	0.17	0.16
	PBE (Ref. 19)	1.69	n.a.	n.a.
	mBJ (this work)	2.93	0.26	0.24
	mBJ (Ref. 11)	2.88	n.a	n.a
	HSE (this work $\alpha = 0.25$)	2.80	0.21	0.17
	HSE (this work $\alpha = 0.30$)	3.03	0.21	0.17
	HSE (Ref. 15 $\alpha = 0.31$)	3.48	0.22	0.19
	Exp. (Ref. 21)	3.50	0.18–0.29	0.18–0.29
w-AlN	PBE (this work)	4.08	0.30	0.28
	PBE $2 \times 2 \times 2$ SC (this work)	4.08	0.30	0.28
	PBE (Ref. 11)	4.09	n.a.	n.a.
	PBE (Ref. 19)	4.02	n.a.	n.a.
	mBJ (this work)	5.51	0.40	0.37
	mBJ (Ref. 11)	5.57	n.a	n.a.
	HSE (this work $\alpha = 0.25$)	5.41	0.34	0.33
	HSE (this work $\alpha = 0.30$)	5.68	0.31	0.31
	HSE (Ref. 15 $\alpha = 0.31$)	6.04	0.32	0.30
	Exp. (Ref. 21)	6.28	0.29–0.45	0.29–0.45

used to efficiently calculate the band structure. The energy gap and the effective masses have been reported in Table II and compared with previous works based on DFT simulations and experiments. As expected, calculations performed with the PBE approximations provide a strong underestimation of the energy gap E_g. On the contrary, a good agreement has been found between mBJ-PBE and HSE, which, in terms of E_g, are closer to the corresponding experimental values.[11] As far as the calculation of the effective masses is concerned, it has been found that the HSE approach provides the most accurate results when compared with experimental data,[19] while mBJ meta-GGA overestimates them along both the monitored crystalline orientations. In contrast, PBE provides good results for w-AlN while slightly underestimates m^* for w-GaN.[20] The PBE potential has been then chosen as the most suitable approximation of the exchange-correlation term in the Kohn–Sham equations for the following reasons: (i) it is a full *ab initio* method since there are no fitting parameters, (ii) it has a lower computational cost when compared to mBJ and, especially, to HSE, and (iii) the error on the effective masses is similar or even lower then the mBJ one.

IV. AlGaN AND ScAlN ALLOYS

In order to check the consistency of the simulation setup, the fully relaxed band structure of $2 \times 2 \times 2$ SCs of w-GaN and w-AlN has been calculated and compared with the PC calculations reported above. As expected, no differences in the energy gap and effective masses have been found. Moreover, the observed differences on the lattice constants can be considered negligible. Thus, simulations of the two alloys under investigation have been carried out. The EBS of $Al_xGa_{1-x}N$ and $Sc_xAl_{1-x}N$ for four different values of x is reported in Figs. 1 and 2, respectively. Since both AlN and GaN are stable in the wurtzite phase, the increase of disorder in $Al_xGa_{1-x}N$ is small in the whole composition range; thus, the unfolding procedure can be successfully applied. The corresponding lattice parameters as a function of x are reported in Table III showing an approximately linear decrease with x (Vegard's law). The same considerations apply to the electron effective masses and to the energy gap as shown in Fig. 3. On the contrary, ScN is stable

Downloaded from http://pubs.aip.org/aip/jap/article-pdf/doi/10.1063/5.0115512/16521706/215108_1_online.pdf

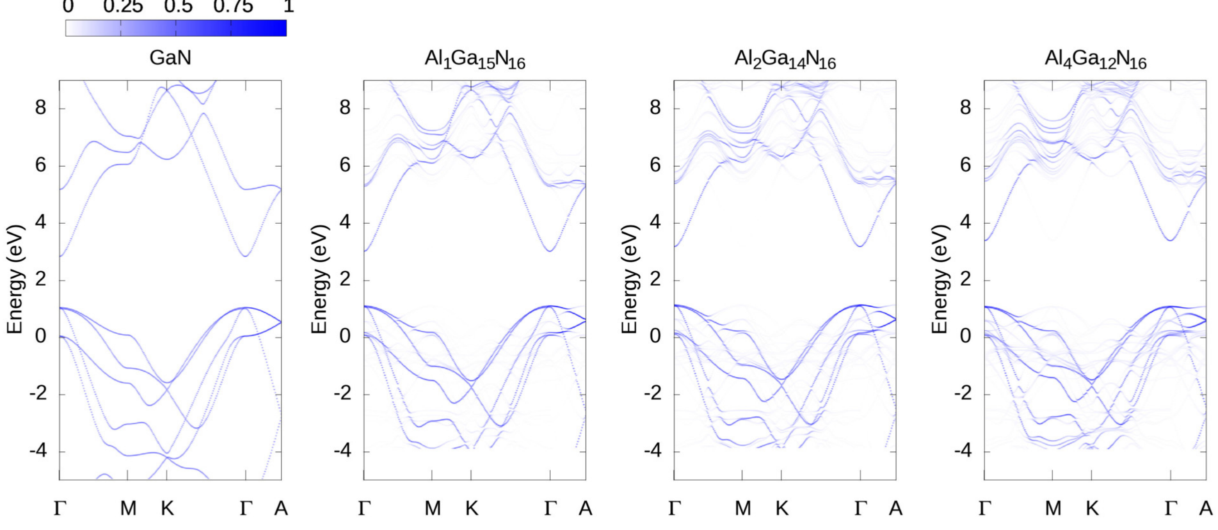

FIG. 1. EBS of $Al_xGa_{1-x}N$ for different Al concentrations (x = 0, 0.0625, 0.125, 0.25).

© Author(s) 2022

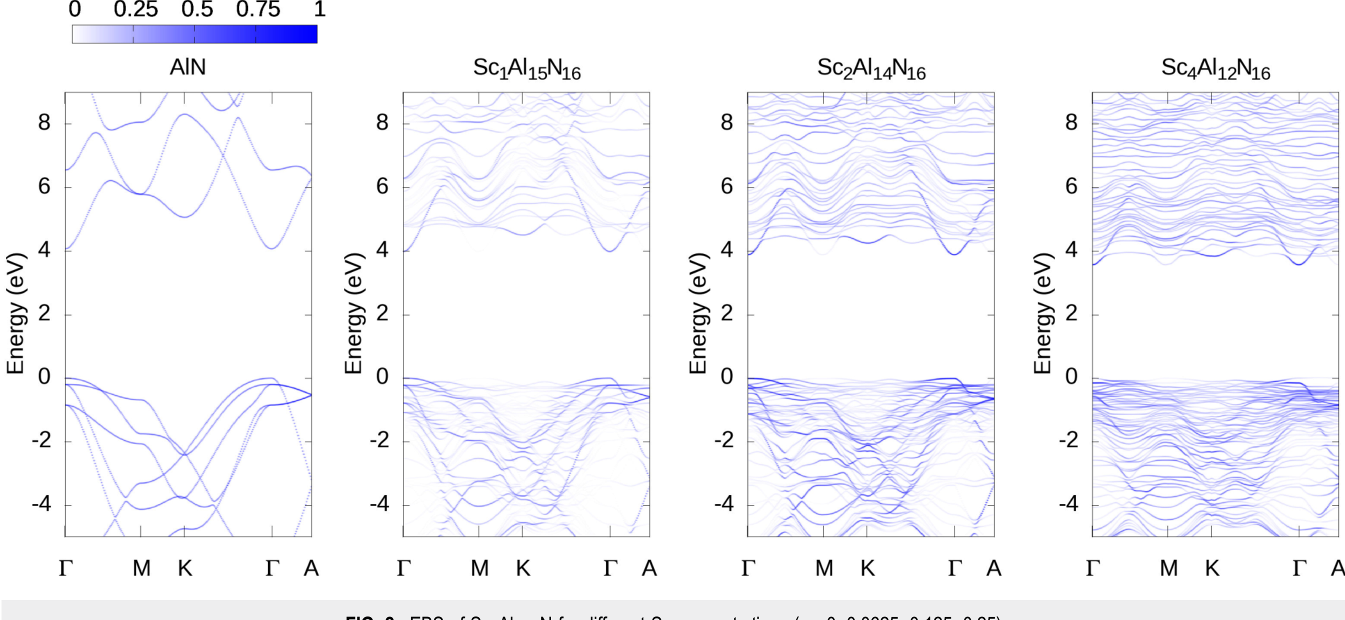

FIG. 2. EBS of $Sc_xAl_{1-x}N$ for different Sc concentrations (x = 0, 0.0625, 0.125, 0.25).

in the rock-salt phase. For this reason, in $Sc_xAl_{1-x}N$, the amount of disorder strongly increases with x making useless the concept of EBS for high Sc concentrations. The DFT calculations of $Sc_xAl_{1-x}N$ correspond to w-AlN for $x = 0$ and to layered-hexagonal ScN (lh-ScN) for $x = 1$ with the internal parameter u [that characterizes the distance between the (0001) planes containing metal atoms and N atoms] fixed to $u = 0.5$. The latter structure is unstable, and the equilibrium crystal structure of ScN is cubic rock-salt. However, the Sc–N bond lengths in lh-ScN are very close to the one of cubic rock-salt ScN.[22] The calculated lattice parameters are reported in Table III. In Fig. 4, the ScAlN lattice parameters are compared with those of Ref. 11 showing good agreement. The Vegard law can be applied on a for $0 \leq x \leq 0.50$,[11] while it is not valid for c since it is a non-monotonic function of x. However, if $x \leq 0.25$, the conduction band minimum is still located in the Γ-point and the corresponding value of the spectral weights[7–9] are close to 1. Therefore, it is still possible to extract m^* around the Γ point. It is worth nothing that, for RF and power electronic applications, the adopted Sc concentration ranges between $x = 10\%$ and

TABLE III. Calculated lattice parameter a and c of $Sc_xAl_{1-x}N$ and $Al_xGa_{1-x}N$. 0 (PC) corresponds to calculations on a single cell with $x = 0$, and 0 (SC) corresponds to calculations on the corresponding supercell.

	$Sc_xAl_{1-x}N$		$Al_xGa_{1-x}N$	
x	a (Å)	c (Å)	a (Å)	c (Å)
0 (PC)	3.1269	5.0129	3.2129	5.2332
0 (SC)	3.1267	5.0132	3.2123	5.2343
0.0625	3.1534	5.0356	3.2072	5.2221
0.125	3.1797	5.0547	3.2013	5.2090
0.1875	3.1994	5.0900	n.a.	n.a.
0.25	3.2409	5.0875	3.1894	5.1836
0.50	n.a.	n.a.	3.1675	5.1311
0.75	n.a.	n.a.	3.1469	5.0741
1	n.a.	n.a.	3.1267	5.0132

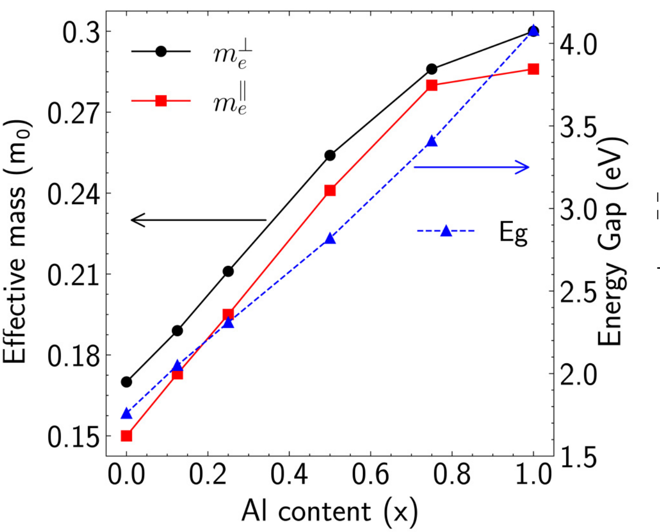

FIG. 3. Electron effective masses and the energy gap of $Al_xGa_{1-x}N$ as a function of the Al concentration.

Downloaded from http://pubs.aip.org/aip/jap/article-pdf/doi/10.1063/5.0115512/16521706/215108_1_online.pdf

© Author(s) 2022

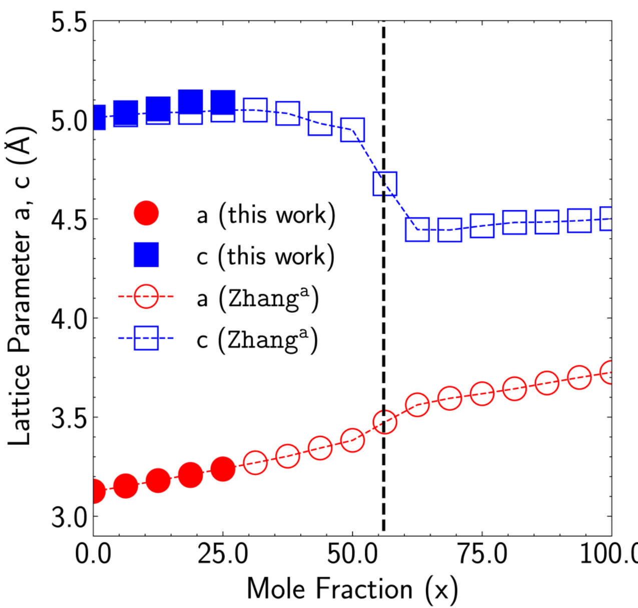

FIG. 4. Lattice constants of $Sc_xAl_{1-x}N$ as a function of the Sc content compared with the previous work in the literature. The black vertical dashed line indicates the transition from wurtzite to an unstable layered-hexagonal phase.

$x = 26\%$.[4,23,24] Thus, the present analysis is sufficient to guarantee an accurate estimation of the electron effective masses for TCAD simulations of Sc-based HEMTs. In Fig. 5, the energy gap and the electron effective masses are reported as functions of x. As expected, the energy gap decreases with x, while an anomalous behavior of both masses $m^{\parallel}$ and $m^{\perp}$ has been found. Along the $\Gamma \rightarrow M$ direction, $m^{\perp}$ slightly decreases in the range $0 \leq x \leq 0.1875$, while it significantly increases at $x = 0.25$. The opposite is true along the $\Gamma \rightarrow A$ direction for $m^{\parallel}$. The electron effective masses of AlGaN and ScAlN are mostly affected by two factors: the variation of the chemical composition and the consequent alteration of the crystal structure. In AlGaN, both these phenomena result in an increase of m^* with x, leading to the Vegard law. In order to gain a physical insight on the role played by the Sc concentration on m^*, two different sets of simulations have been performed: (i) calculation of the ScAlN band structure without performing relaxation (with lattice constants and atomic positions of w-AlN) and (ii) calculation of the AlN band structure using lattice constants and atomic positions from the variable-cell relaxation of the $Sc_xAl_{1-x}N$. The electron effective masses along both the $\Gamma - M$ and $\Gamma - A$ directions have been calculated and reported in Fig. 6. It has been found that the presence of Sc atoms leads to an increase of m^* in both directions. Vice versa, the increase of the lattice constants a and c along with the internal parameter u reduces m^*. The superposition of these two phenomena leads to the observed dependence of the effective mass on x in Fig. 5.

Differently from w-AlN, where the second lowest-lying minimum of the conduction band is located along the M–L direction, in ScAlN, it is found to be in the K-point, and as x increases, it moves toward lower energies (Fig. 2). This is clearly correlated with the transition from a direct to an indirect gap ($\Gamma \rightarrow K$). For $x = 1$ (lh-ScN), the conduction band minimum is located in the K-point of the Brillouin and can be mostly ascribed to d-orbitals of Sc atoms.[25] By increasing x, the number of states provided by such orbitals increase, and due to lattice deformation toward a layered-hexagonal crystal structure, the K-point minimum moves toward lower energies. As shown in Fig. 7, the DOS corresponding to different values of x is

Downloaded from http://pubs.aip.org/aip/jap/article-pdf/doi/10.1063/5.0115512/16521706/215108_1_online.pdf

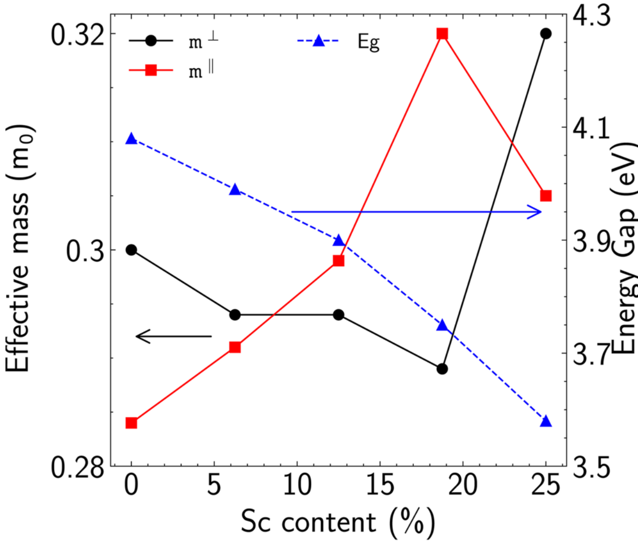

FIG. 5. Electron effective masses and energy gap of $Sc_xAl_{1-x}N$ as a function of the Sc concentration.

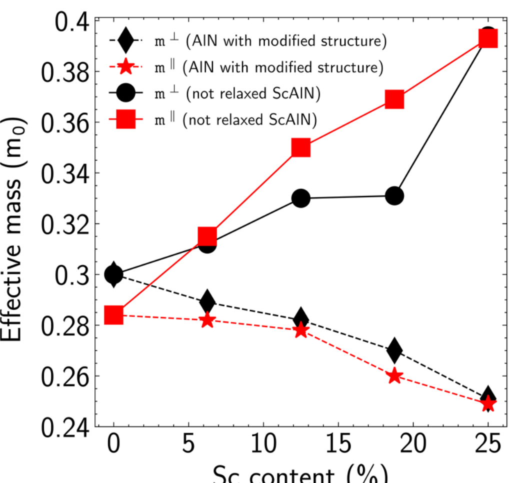

FIG. 6. Solid lines: electron effective masses of ScAlN as a function of x calculated without performing variable-cell relaxation. Dashed lines: electron effective masses extracted from simulation of $2 \times 2 \times 2$ AlN SC performed using lattice constants and atomic positions from variable-cell relaxation of ScAlN.

© Author(s) 2022

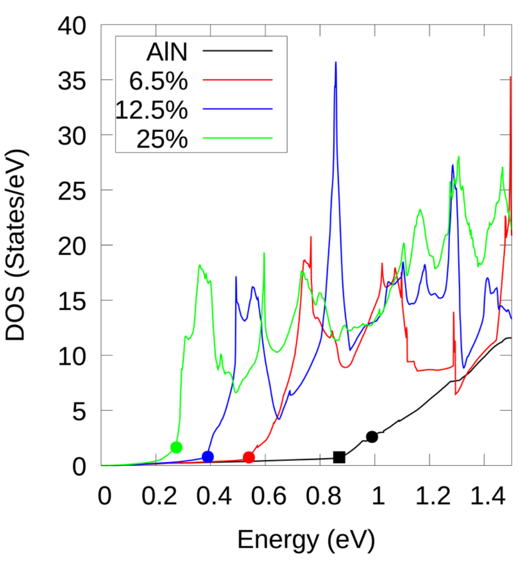

FIG. 7. Density of states of $Sc_xAl_{1-x}N$ for different values of the Sc concentration (x = 0, 0.0625, 0.125, 0.25). Dots show the value of the energy corresponding to the minimum of the conduction band in the K-point extracted from the EBS. Black square: value of the energy corresponding to the minimum of the conduction band along the M–L direction extracted from the w-AlN EBS.

significantly influenced by the change of the local minimum in the K-point, leading to a shift of the corresponding DOS peak, which might influence the high-energy transport properties.

V. CONCLUSION

In this paper, first-principles calculations of the electron effective masses of $Al_xGa_{1-x}N$ and $Sc_xAl_{1-x}N$ have been performed using the unfolding technique. It has been confirmed that in $Al_xGa_{1-x}N$, the wurtzite crystal structure is approximately preserved independently on x. For this reason, both E_g and m^* linearly increase with the Al concentration. On the contrary, in $Sc_xAl_{1-x}N$, the amount of disorder strongly increases with x; thus, the effective band structure can be extracted only for $0 \leq x \leq 0.25$. In this range, the lattice constants c and a are non-monotonic functions of x. In addition, the minimum in the K valley moves toward lower energies, leading to new peaks in the density of states. To conclude, the present analysis gives an accurate estimation of the electron effective mass of $Al_xGa_{1-x}N$ and $Sc_xAl_{1-x}N$ as functions of x in the most interesting ranges of values for future applications. In the former case, the Vegard law can be adopted to nicely predict the linear change of m^*. In the latter one, DFT simulations are required to calculate m^*, which is a fundamental ingredient to perform accurate TCAD analyses of HEMTs for power and RF applications at the design stage.

ACKNOWLEDGMENTS

This research was partially funded by the EC project GAN4AP (G.A. 101007310) via the IUNET Consortium.

AUTHOR DECLARATIONS

Conflict of Interest

The authors have no conflicts to disclose.

Author Contributions

Luigi Balestra: Conceptualization (equal); Data curation (lead); Methodology (equal); Validation (lead); Visualization (lead); Writing – original draft (lead). **Elena Gnani:** Conceptualization (equal); Methodology (equal); Validation (supporting); Writing – review & editing (supporting). **Susanna Reggiani:** Funding acquisition (lead); Methodology (equal); Supervision (lead); Validation (supporting); Writing – review & editing (supporting).

DATA AVAILABILITY

The data that support the findings of this study are available from the corresponding author upon reasonable request.

REFERENCES

[1]J. Fang, M. V. Fischetti, R. D. Schrimpf, R. A. Reed, E. Bellotti, and S. T. Pantelides, "Electron transport properties of $Al_xGa_{1-x}N$/GaN transistors based on first-principles calculations and Boltzmann-equation Monte Carlo simulations," Phys. Rev. Appl. **11**, 044045 (2019).

[2]K. Furuta, K. Hirata, S. A. Anggraini, M. Akiyama, M. Uehara, and H. Yamada, "First-principles calculations of spontaneous polarization in ScAlN," J. Appl. Phys. **130**, 024104 (2021).

[3]M. T. Hardy, B. P. Downey, N. Nepal, D. F. Storm, D. S. Katzer, and D. J. Meyer, "Epitaxial ScAlN grown by molecular beam epitaxy on GaN and SiC substrates," Appl. Phys. Lett. **110**, 162104 (2017).

[4]A. J. Green, J. K. Gillespie, R. C. Fitch, D. E. Walker, M. Lindquist, A. Crespo, D. Brooks, E. Beam, A. Xie, V. Kumar, and J. Jimenez, "ScAlN/GaN high-electron-mobility transistors with 2.4 A/mm current density and 0.67 S/mm transconductance," IEEE Electron Device Lett. **40**, 1056–1059 (2019).

[5]C. Manz, S. Leone, L. Kirste, J. Ligl, K. Frei, T. Fuchs, M. Prescher, P. Waltereit, M. A. Verheijen, A. Graff, and M. Simon-Najasek, "Improved AlScN/GaN heterostructures grown by metal-organic chemical vapor deposition," Semicond. Sci. Technol. **36**, 034003 (2021).

[6]S. M. Sze, Y. Li, and K. K. Ng, *Physics of Semiconductor Devices* (John Wiley & Sons, 2021).

[7]W. Ku, T. Berlijn, and C.-C. Lee, "Unfolding first-principles band structures," Phys. Rev. Lett. **104**, 216401 (2010).

[8]V. Popescu and A. Zunger, "Effective band structure of random alloys," Phys. Rev. Lett. **104**, 236403 (2010).

[9]V. Popescu and A. Zunger, "Extracting E versus $\vec{k}$ effective band structure from supercell calculations on alloys and impurities," Phys. Rev. B **85**, 085201 (2012).

[10]N. Pant, Z. Deng, and E. Kioupakis, "High electron mobility of $Al_xGa_{1-x}N$ evaluated by unfolding the DFT band structure," Appl. Phys. Lett. **117**, 242105 (2020).

[11]S. Zhang, D. Holec, W. Y. Fu, C. J. Humphreys, and M. A. Moram, "Tunable optoelectronic and ferroelectric properties in Sc-based III-nitrides," J. Appl. Phys. **114**, 133510 (2013).

[12]P. Giannozzi, O. Andreussi, T. Brumme, O. Bunau, M. B. Nardelli, M. Calandra, R. Car, C. Cavazzoni, D. Ceresoli, M. Cococcioni, and N. Colonna, "Advanced capabilities for materials modelling with quantum ESPRESSO," J. Phys.: Condens. Matter **29**, 465901 (2017).

[13]J. P. Perdew, K. Burke, and M. Ernzerhof, "Generalized gradient approximation made simple," Phys. Rev. Lett. **77**, 3865 (1996).

Downloaded from http://pubs.aip.org/aip/jap/article-pdf/doi/10.1063/5.0115512/16521706/215108_1_online.pdf

© Author(s) 2022

[14]A. Van de Walle, P. Tiwary, M. De Jong, D. Olmsted, M. Asta, A. Dick, D. Shin, Y. Wang, L.-Q. Chen, and Z.-K. Liu, "Efficient stochastic generation of special quasirandom structures," Calphad **42**, 13–18 (2013).
[15]C. Dreyer, A. Janotti, and C. Van de Walle, "Effects of strain on the electron effective mass in GaN and AlN," Appl. Phys. Lett. **102**, 142105 (2013).
[16]P. E. Blöchl, O. Jepsen, and O. K. Andersen, "Improved tetrahedron method for Brillouin-zone integrations," Phys. Rev. B **49**, 16223 (1994).
[17]J. Heyd, G. E. Scuseria, and M. Ernzerhof, "Hybrid functionals based on a screened Coulomb potential," J. Chem. Phys. **118**, 8207–8215 (2003).
[18]G. Pizzi, V. Vitale, R. Arita, S. Blügel, F. Freimuth, G. Géranton, M. Gibertini, D. Gresch, C. Johnson, T. Koretsune, J. Ibañez-Azpiroz, H. Lee, J.-M. Lihm, D. Marchand, A. Marrazzo, Y. Mokrousov, J. I. Mustafa, Y. Nohara, Y. Nomura, L. Paulatto, S. Poncé, T. Ponweiser, J. Qiao, F. Thöle, S. S. Tsirkin, M. Wierzbowska, N. Marzari, D. Vanderbilt, I. Souza, A. A. Mostofi, and J. R. Yates, "Wannier90 as a community code: New features and applications," J. Phys.: Condens. Matter **32**, 165902 (2020).
[19]P. G. Moses, M. Miao, Q. Yan, and C. G. Van de Walle, "Hybrid functional investigations of band gaps and band alignments for AlN, GaN, InN, and InGaN," J. Chem. Phys. **134**, 084703 (2011).
[20]Q. Yan, E. Kioupakis, D. Jena, and C. G. Van de Walle, "First-principles study of high-field-related electronic behavior of group-III nitrides," Phys. Rev. B **90**, 121201 (2014).
[21]I. Vurgaftman and J. N. Meyer, "Band parameters for nitrogen-containing semiconductors," J. Appl. Phys. **94**, 3675–3696 (2003).
[22]D. F. Urban, O. Ambacher, and C. Elsässer, "First-principles calculation of electroacoustic properties of wurtzite (Al, Sc) N," Phys. Rev. B **103**, 115204 (2021).
[23]J. Ligl, S. Leone, C. Manz, L. Kirste, P. Doering, T. Fuchs, M. Prescher, and O. Ambacher, "Metalorganic chemical vapor phase deposition of AlScN/GaN heterostructures," J. Appl. Phys. **127**, 195704 (2020).
[24]S.-M. Chen, S.-L. Tsai, K. Mizutani, T. Hoshii, H. Wakabayashi, K. Tsutsui, E. Y. Chang, and K. Kakushima, "GaN high electron mobility transistors (HEMTs) with self-upward-polarized AlScN gate dielectrics toward enhancement-mode operation," Jpn. J. Appl. Phys. **61**, SH1007 (2022).
[25]G. Peng-Fei, W. Chong-Yu, and Y. Tao, "Electronic structure and physical properties of ScN in pressure: Density-functional theory calculations," Chin. Phys. B **17**, 3040 (2008).

Downloaded from http://pubs.aip.org/aip/jap/article-pdf/doi/10.1063/5.0115512/16521706/215108_1_online.pdf

© Author(s) 2022